17. R. K. Morgan, M.S. Cohen. A Clickable Aminooxy Probe for Monitoring Cellular ADP-Ribosylation. *ACS Chem Biol.* **10,** 1778-84 (2015).
18. H. Kleine, E. Poreba, K. Lesniewicz, P.O. Hassa, M.O. Hottiger, *et al.* Substrate-assisted catalysis by PARP10 limits its activity to mono-ADP-ribosylation. *Mol Cell.* **32,** 57-69 (2008).
19. A. Tzur, R. Kafri, V.S. LeBleu, G. Lahav, M.W. Kirschner. Cell growth and size homeostasis in proliferating animal cells. *Science*. **325,** 167-71 (2009).
20. J. Yoshino J and S. Imai. Accurate measurement of nicotinamide adenine dinucleotide (NAD^+) with high-performance liquid chromatography. *Methods Mol Biol.* **1007,** 203-15 (2013).

Materials and Methods:

Sensor construction.

A cDNA fragment encoding the bacterial NAD^+-dependent DNA ligase binding domain was obtained by PCR of genomic DNA of *E. faecalis* (OHSU isolate). Subdomains from cpVenus and the ligase NAD^+ binding domain were PCR amplified with 20nt overlapping ends to facilitate Gibson Assembly into pENTR-6 (modified from pENTR-4 to include additional restriction sites). Point mutations (K44L and D210N) were introduced via site-directed mutagenesis. After sequence validation, the final construct was inserted into lentiviral expression vector pCMV-Flag-HA-CcdB-IRES-puro using Gateway Cloning.

Protein purification.

The sensors and controls were purified in batch format from mammalian HEK293T cells via their N-terminal Flag epitope tag, using anti-Flag M2 Affinity Gel (Sigma) and lysis buffer (50 mM Tris pH 7.4, 150 mM NaCl, 1 mM EDTA, 10 mM NaF, 0.5% NP-40, 1 mM DTT, and Complete Protease Inhibitor cocktail). Protein was eluted with 500 µg/mL 3x Flag peptide and dialyzed against 100 mM Tris pH 7.4, 150 mM NaCl, 0.5 mM DTT, 100 µM PMSF, 1 mM EDTA, and 50% glycerol. Bradford assays were used to quantify the concentration in each batch and aliquots were flash frozen in liquid nitrogen for storage at -80°C.

Fluorescence and absorbance spectroscopy.

Steady-state fluorescence intensity measurements were performed using a Photon Technology International Quanta Master fluorometer. Excitation spectra were monitored at 530 nm and emission spectra were measured by excitation at 488 nm and 405 nm. Slit widths used gave 2 nm bandpass for excitation and 11 nm bandpass for emission. Absorbance spectroscopy was performed on a Shimadzu 1601 spectrophotometer. Temperature was controlled with a water jacket and monitored using an Omega Thermistor.

NAD^+ washout.

Purified sensor (2 µM) was incubated with either 0 µ or 500 µM NAD^+ in a total of 75 µL and evaluated for its fluorescence excitation and emission spectra. Each sample was then passed over a pre-equilabrated (50 mM Tris pH 7.4, 150 mM NaCl) micro buffer exchange column (Bio-Rad Micro Bio-Spin P-30), washed, and eluted in 75 µL buffer volume for reevaluation of fluorescence.

Competition for free NAD^+.

Fluorescence emission of 250 nM purified sensor was monitored at 520 nm following excitation at 488 nm over time. Three 1-second exposures were obtained every 30 seconds at 20°C in 100 mM HEPES pH 7.4, 150 mM NaCl, 10 mM $MgCl_2$. At the 240 second timepoint, NAD^+ was added to a final concentration of 10 µM; at the 600 second timepoint, full-length active human GAPDH (Abcam) was added to a final concentration of 11.7 µM. Fluorescence measurements were corrected for dilution factor. Mean±SD, n=2.

Fluorescence lifetime measurements.
Fluorescence lifetime measurements were performed on a PicoQuant FluoTime 200 time correlated single photon counting instrument (PicoQuant, Berlin), outfitted with a Hamamatsu micro-channel plate detector. Decays were measured with the polarizers at the magic angle and with 16 nm bandpass emission slits. Excitation was achieved using a pulsed diode laser of 485 nm, which yielded an Instrument Response Function (IRF) of 128 ps (FWHM), measured using a Ludox solution. Emission from the samples was collected at 525 nm, with an additional 520 nm long-pass filter on the detector side of the sample. The fluorescence decays were fit by means of PicoQuant software, using an exponential decay model [$I(t) = \sum_{i-1}^{n} A_i e^{-t/\tau_i}$], where A_i is the amplitude of the ith component, in counts, in the first range fitting channel and τ_i is the lifetime of the ith component].

Flow cytometry.
Data was collected on a BD LSRFortessa using 488-1 (ex. 488 nm, em. 525/50 nm) and 405-2 (ex. 405 nm, em. 515/20 nm) for the sensor, and 561-3 (ex. 561 nm, em. 670/30 nm) for PI intensity. Cells were gated to exclude debris, a standard doublet-exclusion was performed, and 1x10^4 fluorescent cells were evaluated per condition. Data were analyzed and plotted with FlowJo X. Ratiometric 488/405 nm fluorescence values were obtained per cell using the derived function on FlowJo X.

Imaging.
Live cell imaging was done on a fully motorized Nikon TiE stand with a Yokogawa W1 spinning disk confocal unit. Instrumentation for this project included a motorized stage in x and y for point-revisiting; z-axis control for fast piezo-based positioning and continuous focus-drift compensation for live cell imaging; dual-pinhole array for improved optical sectioning, a high-powered Agilent laser launch; split simultaneous acquisition on two Andor Zyla 5.5 sCMOS cameras; and a 100x1.49 Apo TIRF objective. During imaging, cells were maintained in 5% CO_2 at 34°C. Cells were excited at 488 nm and monitored with emission 525/25 nm. For each condition, at least 5 fields containing approximately 50-100 cells were used for quantification of pixel intensity using Metamorph software. The mean intensity per field was normalized to the control condition to obtain the normalized intensity measurement. Background was subtracted from each image.

Statistical analysis.
Ratio of ratios: Data were analyzed using a linear mixed-effect model fit by Restricted Maximum Likelihood (REML) with STATA/IC 14 software. Fluorescence intensity was log transformed prior to analysis to help stabilize variance and limit the impact of outliers. P value calculations were performed on the ratio of ratios for $\left(\frac{F_{Sensor}}{F_{SensorScram}}\right)$ / $\left(\frac{F_{cpV}}{F_{cpVScram}}\right)$.

Two-way repeated measurement ANOVA: Analysis was performed using GraphPad Prism6, comparing mean values per column and row. An adjusted p-value from Sidak multiple comparison test was reported.

Statistical calibration estimation of error: The two major variance components ($SD_{replicates}$ and $SD_{lack\ of\ fit}$) reported by GraphPad Prism6 from the sigmoidal regression were used to calculate SDx for the interpolated x value. $2 \times SDx$ was used for the 95% confidence interval (95% CI) and reported as $10^{\,x \pm (2 \times SDx)}$.

Cell permeabilization and calculation of free intracellular NAD⁺.

Cells were permeabilized in the presence of 30 μM propidium iodide with either 0.001% digitonin or 0.004% saponin for adherent HeLa cells, and the indicated amount of NAD^+. For calculation of intracellular NAD+, permeabilized clonal populations of HEK293T cells that stably express either the sensor or cpVenus control were equilibrated at RT for 15 minutes with indicated NAD^+ concentrations, and 488/405 nm fluorescence was measured using the Fortessa flow cytometer. To examine how the HeLa population changed with the degree of permeabilization, cells were evaluated within 5-7 minutes of treatment. Fluorescence from the sensor was normalized to the fluorescence from the corresponding cpVenus control. Values from 10 independent experiments were fit to a sigmoidal regression model using GraphPad Prism6 $y = \min + [\frac{(min - \max)}{1+10^{(logEC50 - x) \times HillSlope}}]$ and 95% confidence intervals were calculated as described above. The mean from 21 independent y measurements of the sensor in the cytoplasm or 19 independent y measurements in the nucleus was interpolated to obtain a value for x. 95% confidence intervals are reported.

Quantitation of NAD^+ fluctuations.

Ratiomentric 488/405 nm fluorescence was measured with flow cytometry in individual cells and normalized to cpVenus and control conditions (*e.g.* untreated or siScramble). This measurement of the percent change was interpolated using GraphPad Prism6 onto an *in vitro* titration curve to obtain NAD^+ concentrations and 95% confidence intervals.

qPCR

Total RNA was extracted from cells using RNeasy (Qiagen) and 1 μg was used as the template for cDNA using random-15mer primers and reverse transcriptase MMLV (Life Technologies). Forty cycles of hot-start quantitative-PCR was performed on a DNAEngine Opticon system (MJ Research) with SYBR green. NAMPT-qPCR-F: agggttacaagttgctgccacc; NAMPT-qPCR-R: ctccaccagaaccgaaggcaat; NMNAT1-qPCR-F: gtggaaagagactctgaaggtgc; NMNAT1-qPCR-R: cttgtgtttcagtccacttcctc; NMNAT2#A-F: agatatggaggtgattgttggtg; NMNAT2#A-R: tttgtatttgcggagtattgagg; NMNAT3-qPCR-F: ggatggagacagtgaaggtgct; NMNAT3-qPCR-R: gtcgagaagagtgccttgccat; GAPDH-e1-F: catgacaactttggtatcgtggaagga; GAPDH-e1-R: cacagtcttctgggtggcagtga.

Antibodies and siRNAs

Antibodies for western blotting and immunofluorescence (IF) were incubated overnight at 4°C in 5% milk TBST (westerns) or 2% BSA, 1% horse serum, 0.1% TritonX-100 in PBS (IF). Dilutions were as follows: anti-NAMPT (Bethyl, 1:10 000); anti-NMNAT1 (Abcam, 1:100); anti-NMNAT2 (Abcam, 1:100); anti-NMNAT3 D10 (SCBT, 1:100); anti-Golgin 245 C13 (SCBT, 1:100).

siRNAs were ordered from the human siGENOME library from Dharmacon (GE Healthcare), except for siScramble. siRNAs (25 nM final) were reverse transfected into cells using RNAiMax

(Life Technologies) following manufacturer's protocols and effects were evaluated 72-96 hours post-transfection. siScramble: gugguccaaccgacuaauacag; siTJAP1: gccggtaccgctcattgagct; siNAMPT #1: #D-004581-01; siNAMPT #2: # D-004581-02; siNMNAT2 #2: D-008573-02; siNMNAT2 #3: D-008573-03; siNMNAT3 #1: D-008688-01; siNMNAT3 #3: D-008688-03; siNMNAT3 #4: D-008688-03.

PARP10 auto-ADP-ribosylation.

HEK293T cell lines were transfected with pCMV-GFP-PARP10. Twenty-four hours post-transfection, cells were treated for 1 hour with AO-alkyne (100 μM) and p-phenylenediamine (PDA, 10 mM) to detect PARP10 cellular activity. Method is reported in (17). Briefly, cell pellets were lysed in 25 mM HEPES pH 7.5, 50 mM NaCl, 10% glycerol, 1% NP-40, and protease inhibitors. 80 μg of whole cell lysate was used for click conjugation of the alkyne-labeled PARP10 with 100 μM biotin-azide (Biotin-PEG3-Azide, Click Chemistry Tools) for 1 hour at room temperature in Click Buffer (100 μM of tris[(1-benzyl-1H-1,2,3-triazol-4-yl)methyl]amine (TBTA), 1 mM CuSO4, 1 mM tris(2-carboxyethyl)phosphine hydrochloride (TCEP•HCl, Thermo Scientific Pierce) in 1X PBS + 1% SDS). Reactions were quenched in protein loading sample buffer and assayed using Western blotting with Streptavidin-HRP (1:3333, Jackson ImmunoResearch) to detect biotinylated GFP-PARP10 and anti-GFP (1:1000 Abcam) for GFP-PARP10 and sensor.

Lactate dehydrogenase activity assay.

Similar numbers of cells from each cell line were collected as pellets and freshly processed using a lactate dehydrogenase activity colorimetric assay kit (BioVision) according to manufacturer's instructions. OD450 nm was measured on a SpectraMax M2 (Molecular Devices) plate reader before and after a 30 minute incubation at 37ºC. NADH standard curve and calculations of lactate dehydrogenase activity (mU/mL) was performed according to manufacturer's directions.

Perchloric acid extraction and HPLC analysis for NAD^+.

Cells from each line were collected as on ice and immediately processed with 10% perchloric acid and neutralized with 3 M K_2CO_3, following *(20)*. Samples (10 μL) were analyzed using an Agilent 1100 series HPLC (Santa Clara, CA) with a diode array detector using a sample wavelength of 261 nm and reference wavelength of 360 nm. A gradient mobile phase was delivered at a flow rate of 1.0 ml/min and consisted of two solvents, 50 mM sodium phosphate buffer, pH=6.8, in water (A), and methanol (B). The initial concentration of B was 0%, held for 5 min and then followed by an increase to 5% B over 1 min, held at 5% B for 5 min, then followed by an increase to 15% B over 1 min, held at 15% B for 3 min and returned to start conditions of 0% B in 1 min. The column was equilibrated for 9 min before the next injection. Analytes were separated on a Thermo BetaBasic-18 125x4 mm, 5 μ column with a Betabasic C18 pre-column (10x2.1mm 5 μ) maintained at 30 °C using an Agilent column oven. Instrument control and data were acquired and analyzed using Agilent Chem32 software.

A

B

MEKAPHDIPMYSLNDGFSKEDIFAFDERVRKAIGKPVAYCCELLIDGLAISLRYENGVFVRGATRGDGTVG
ENITENLRTVRSVPMRLTEPISVEVRGECYMPKQSFVALNEEREENGQDIFANPRNAAAGSLRQLDTKIVA
KRNLNTFLYTVADFGPMKAKTQFEALEELSAIGFRTNPERQLCQSIDEVWAYIEEYHEKRSTLPYEINGIV
IKVNEFALQDELGFTVKAPRWAIAYKFPYNSDNVYITADKQKNGIKANFKIRHNIEDGGVQLADHYQQNTP
IGDGPVLLPDNHYLSFQSKLSKDPNEKRDHMVLLEFVTAAGITLGMDELYKGGSGGMVSKGEELFTGVVPI
LVELDGDVNGHKFSVSGEGEGDATYGKLTLKLICTTGKLPVPWPTLVTTLGYGLQCFARYPDHMKQHDFFK
SAMPEGYVQERTIFFKDDGNYKTRAEVKFEGDTLVNRIELKGIDFKEDGNILGHKLEYNGTIVLEGTRSEQ
QPLTLTAATTRAQELRKQLNQYSHEYYVKDQPSVEDYVYDRLYKELVDIETEFPDLITPDSPTQRVG

cpVenus, GGSGG linker
Linker
K44L
D210N

C

Sensor N-terminal variants used in this study:
Flag-epitope tag
HA-epitope tag
Nuclear localization signal from SV40
Cytoplasmic localization signal from MAPKK
Mitochondrial matrix localization signal from COX4

1. MDYKDDDDKLDGGYPYDVPDYAARGYQTSLYKKAGSTMGH
2. MTGPKKKRKVDYKDDDDKLDGGYPYDVPDYAARGYQTSLYKKAGSTMGH
3. MTGLQKKLEELELDDYKDDDDKLDGGYPYDVPDYAARGYQTSLYKKAGSTMGH
4. MLATRVFSLVGKRAISTSVCVRAHTGDYKDDDDKLDGGYPYDVPDYAARGYQTSLYKKAGSTMGH

Fig. S1. Sequence and molecular organization of NAD⁺ sensor.

A) NAD⁺ sensor: K44 is the adenylation site; D210 is predicted to facilitate nucleophilic attack on the α-phosphate group of NAD⁺. We determined empirically that in the context of the sensor, mutations K44L and D210N conferred reversible NAD⁺ binding and shifted the apparent K_d of the sensor into the physiological range.

B) Primary amino acid (aa) sequence of the sensor.

C) N-terminal sequence variants used in this study. These sequences were used to purify the sensor and localize it to specific subcellular compartments.

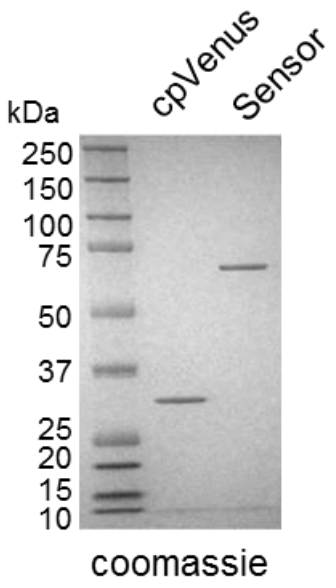

Fig. S2. Coomassie-stained SDS-PAGE of purified cpVenus control and NAD^+ sensor.
The higher molecular weight of the sensor is as expected based on the included NAD^+ binding-domain.

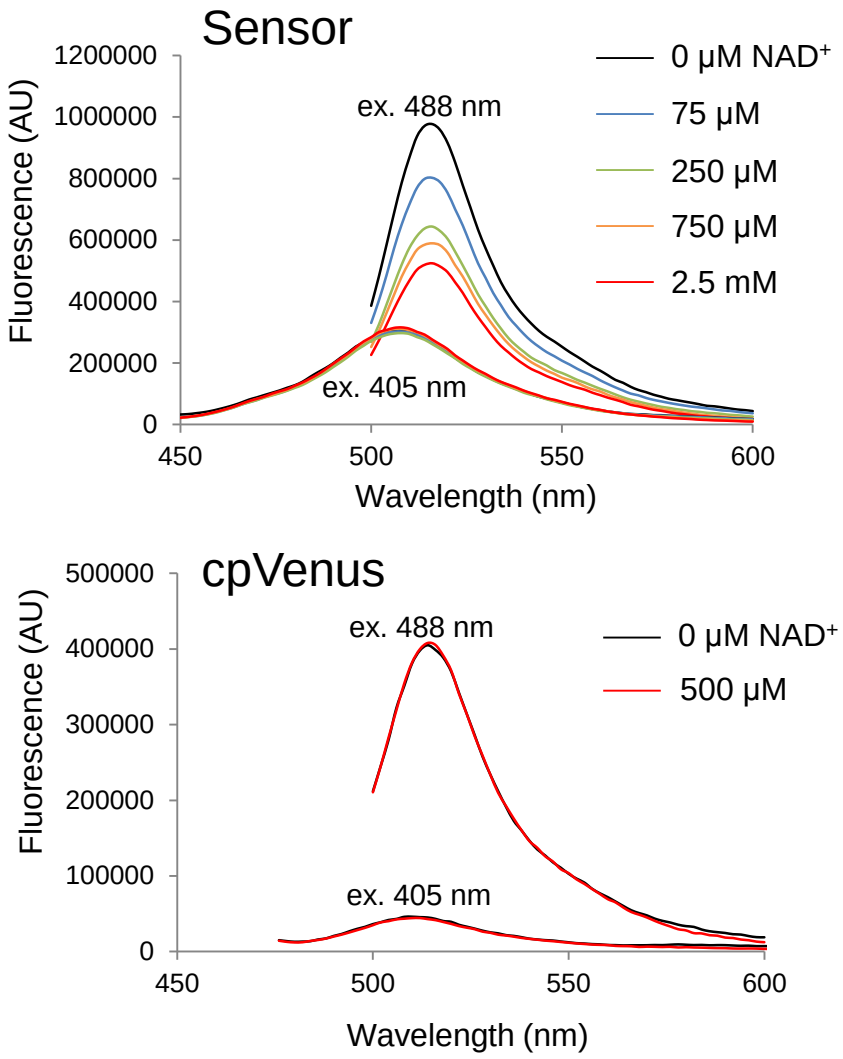

Fig. S3. Emission profiles of the NAD⁺ sensor and cpVenus.
Purified sensor or cpVenus (250 nM) were incubated with indicated amounts of NAD⁺ and excited either at 405 nm or 488 nm. Fluorescence was monitored from 450-600 nm or 500-600 nm, respectively.

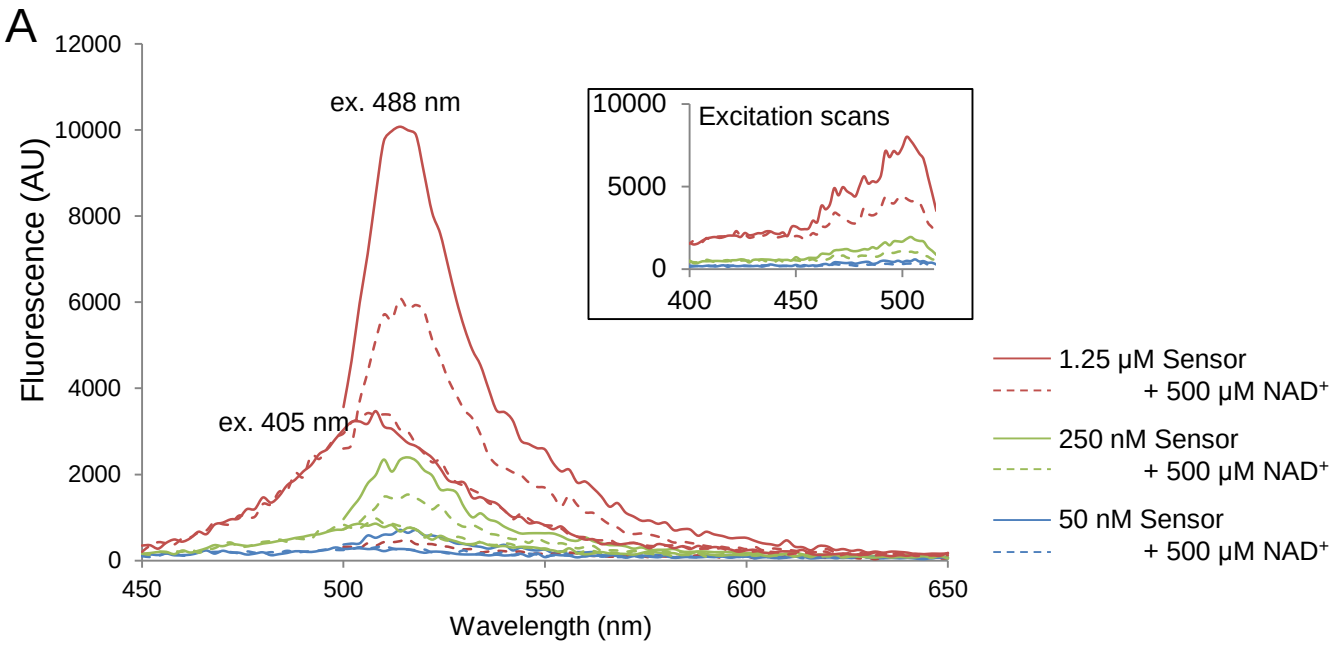

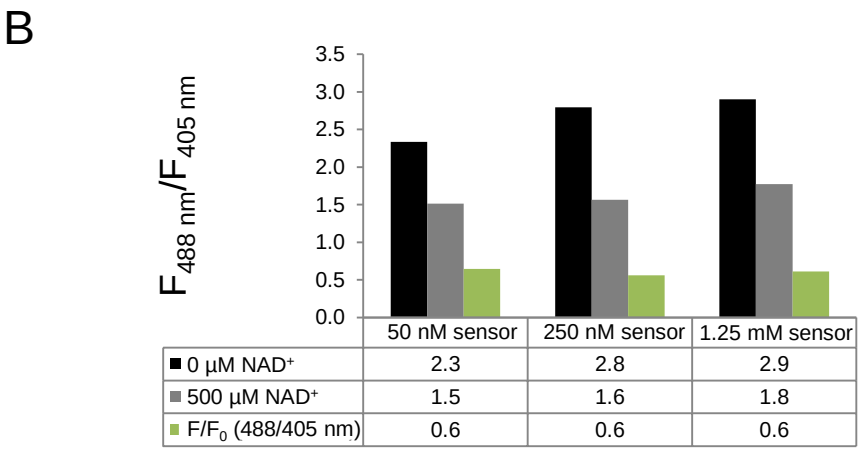

	50 nM sensor	250 nM sensor	1.25 mM sensor
0 µM NAD+	2.3	2.8	2.9
500 µM NAD+	1.5	1.6	1.8
F/F0 (488/405 nm)	0.6	0.6	0.6

Fig. S4. Fluorescence following 405 nm excitation reflects amount of sensor.

A) Amount of sensor was varied as indicated. Fluorescent emission and excitation (inset) scans were obtained with either 0 µM (solid) or 500 µM (dashed) NAD^+.

B) The ratio of 488/405 nm fluorescence for the sensor at different concentrations and 0 µM NAD^+ (black). The 488/405 nm ratio at different concentrations with 500 µM NAD^+ (grey). The NAD^+-dependent change reflected by the 488/405 nm ratio (green).

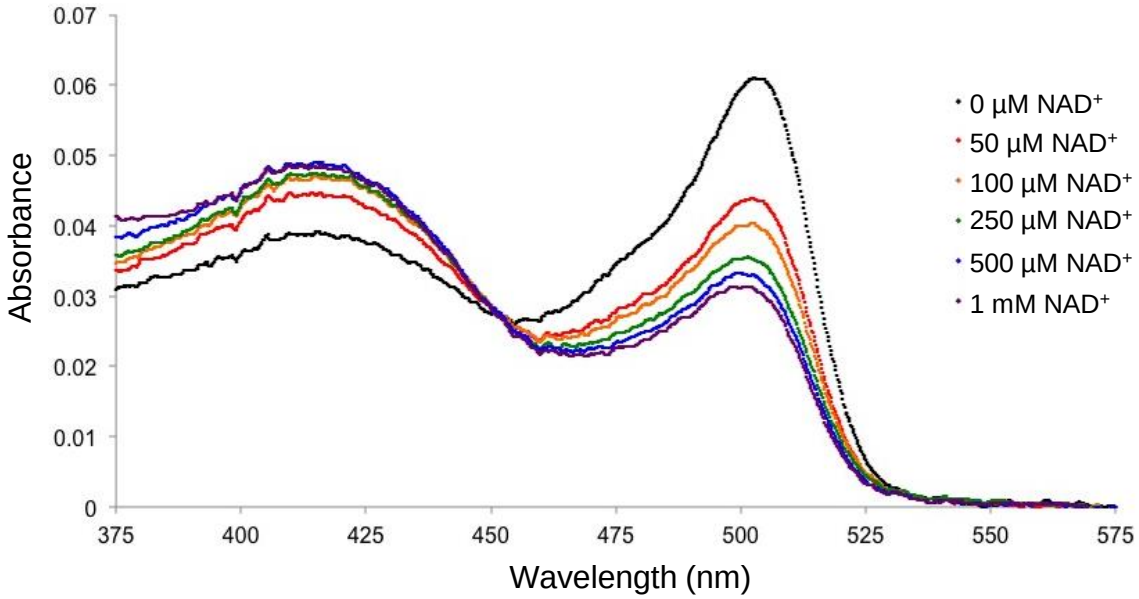

Fig. S5. Absorbance scans of the NAD⁺ sensor.
Purified sensor (5 µM) was incubated with indicated amounts of NAD⁺ (100 mM Tris pH 7.4, 150 mM NaCl @ 20°C) and absorbance was measured from 360-700 nm. Apparent isosbesic point at ~452 nm.

A

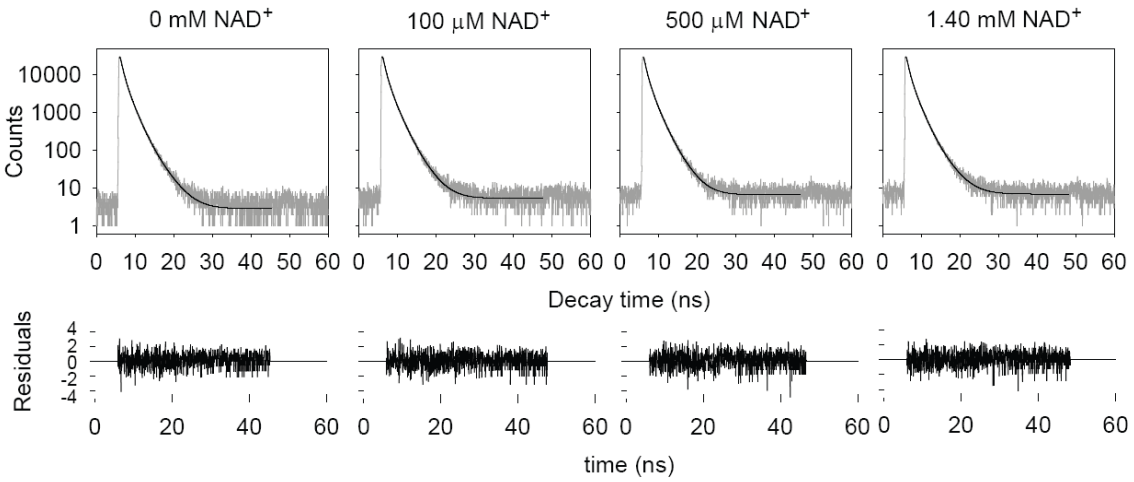

B

NAD^+ [mM]	τ_1	A_1	τ_2	A_2	τ_3	A_3	$\langle\tau\rangle$ (ns)	χ^2	Integration time (s)
0	3.02	1640	1.49	17900	0.567	31300	0.970	0.858	52.0
0.100	2.84	2290	1.47	18900	0.518	30300	0.970	0.914	86.2
0.500	2.70	2770	1.37	19000	0.487	30400	0.929	0.959	107
1.40	3.05	1850	1.49	18400	0.531	30900	0.968	0.945	117

Fig. S6. Lifetime measurements using 488 nm excitation are independent of NAD^+.

A) Fluorescence decays of 250 nM sensor (Ex. 488 nm) were collected up to 30 000 counts in the peak channel and fit with a three-exponential decay function using Fluofit software. Weighted residuals are shown for each fit (bottom).

B) Decays were fit with an exponential decay model [$I(t) = \sum_{i-1}^{n} A_i e^{-t/\tau_i}$]. τ_i is the lifetime of the i^{th} component. A_i is the amplitude of the i^{th} component. $\langle\tau\rangle$ is the amplitude-weighted average lifetime. The increasingly longer integration time required to reach 30,000 counts in the peak channel with increasing NAD^+ concentration indicates less fluorescent species are present in the sample.

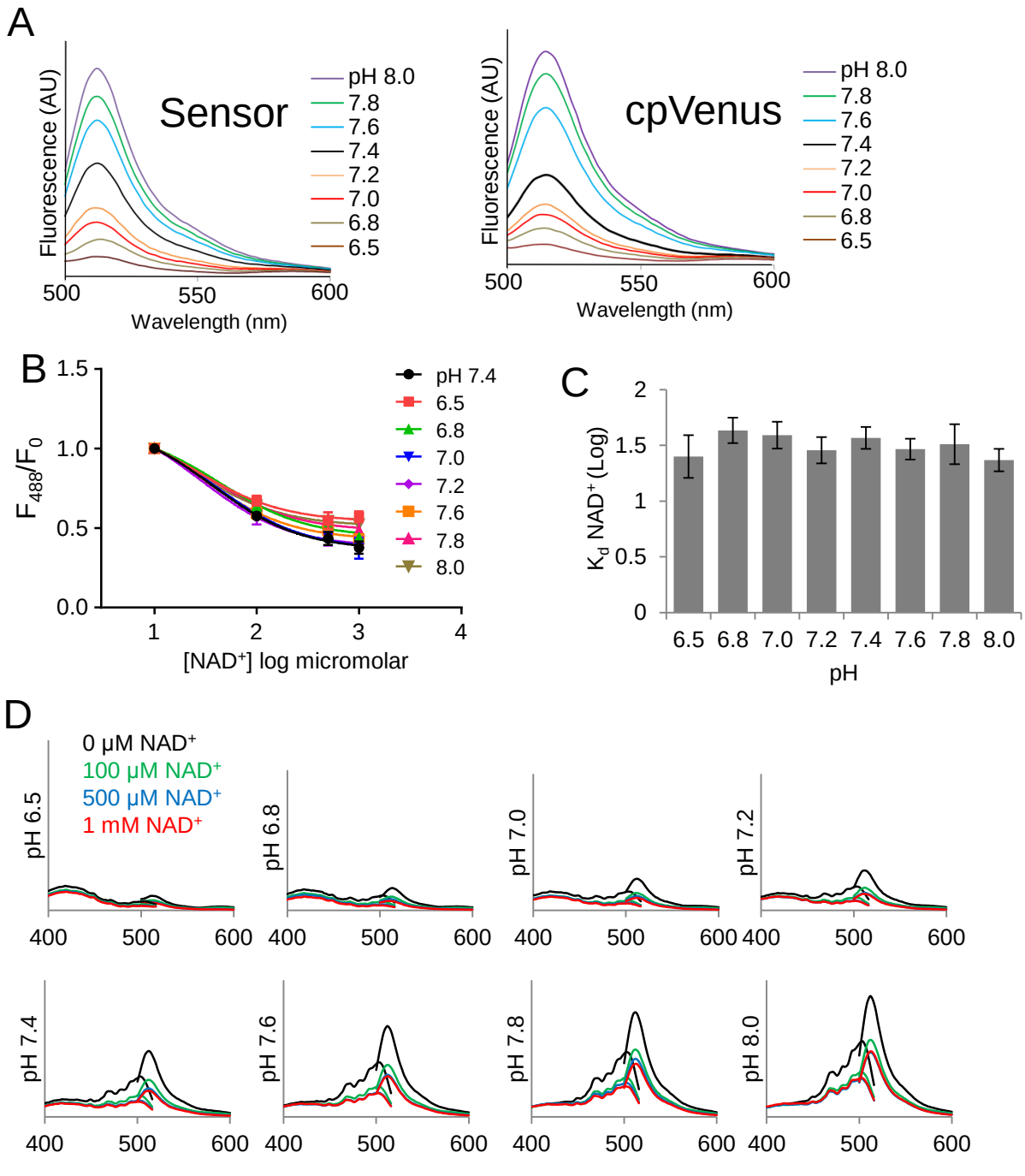

Fig. S7. Effects of pH.

A) Fluorescence (ex. 488 nm) from 250 nM of either the sensor or cpVenus in 100 mM HEPES, 150 mM NaCl at the indicated pH (20°C).

B) Maximum fluorescence (ex. 488 nm) at indicated pH and NAD^+ concentrations, mean±SD, n=3.

C) Comparison of $K_d(NAD^+)$ log values for the sensor at indicated pHs. mean±SD, n=3.

D) Representative excitation (em. 530 nm) and emission (ex. 488 nm) scans are shown at indicated pH and NAD^+ concentrations.

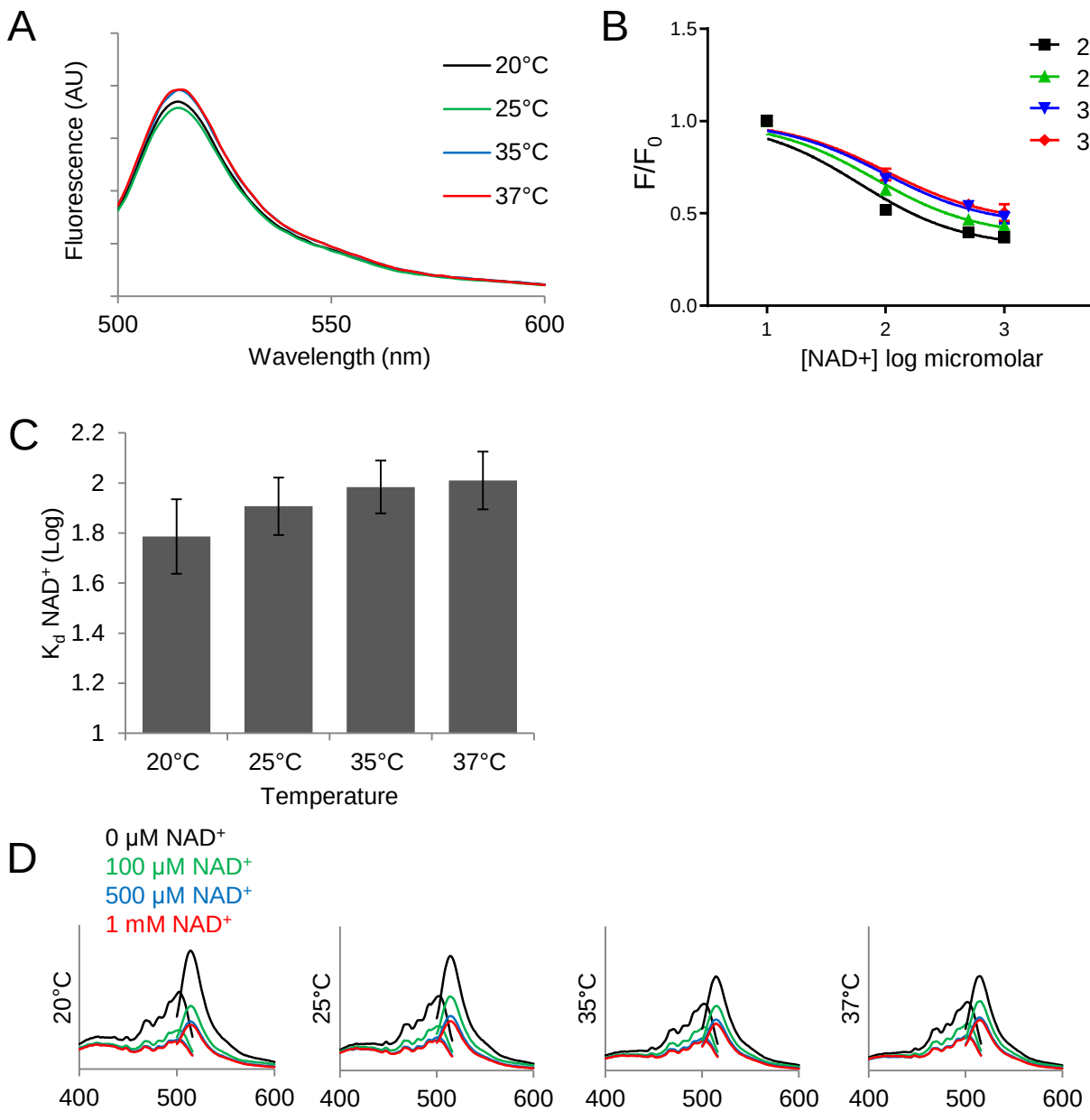

Fig. S8. Effects of temperature.

A) Fluorescence (ex. 488 nm) from 250 nM sensor in 100 mM HEPES, 150 mM NaCl at the indicated temperature.

B) Maximum fluorescence (ex. 488 nm) at indicated temperatures and NAD^+ concentrations, mean±SD, n=2.

C) Comparison of $K_d(NAD^+)$ log values for the sensor at indicated temperatures. mean±SD, n=2.

D) Representative excitation (em. 530 nm) and emission (ex.488 nm) scans at indicated temperatures and NAD^+ concentrations.

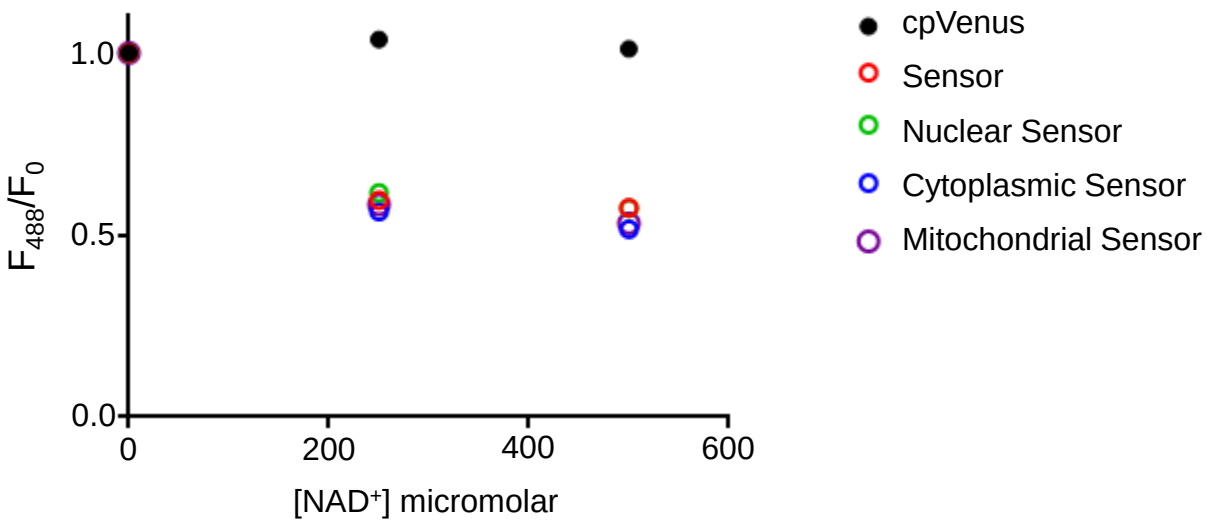

Fig. S9. Localization tags did not affect sensor response to NAD$^+$.
Purified sensors with localization sequences were compared to the original sensor *in vitro*. Relative fluorescence intensity following excitation at 488 nm were plotted as a function of NAD$^+$ concentration.

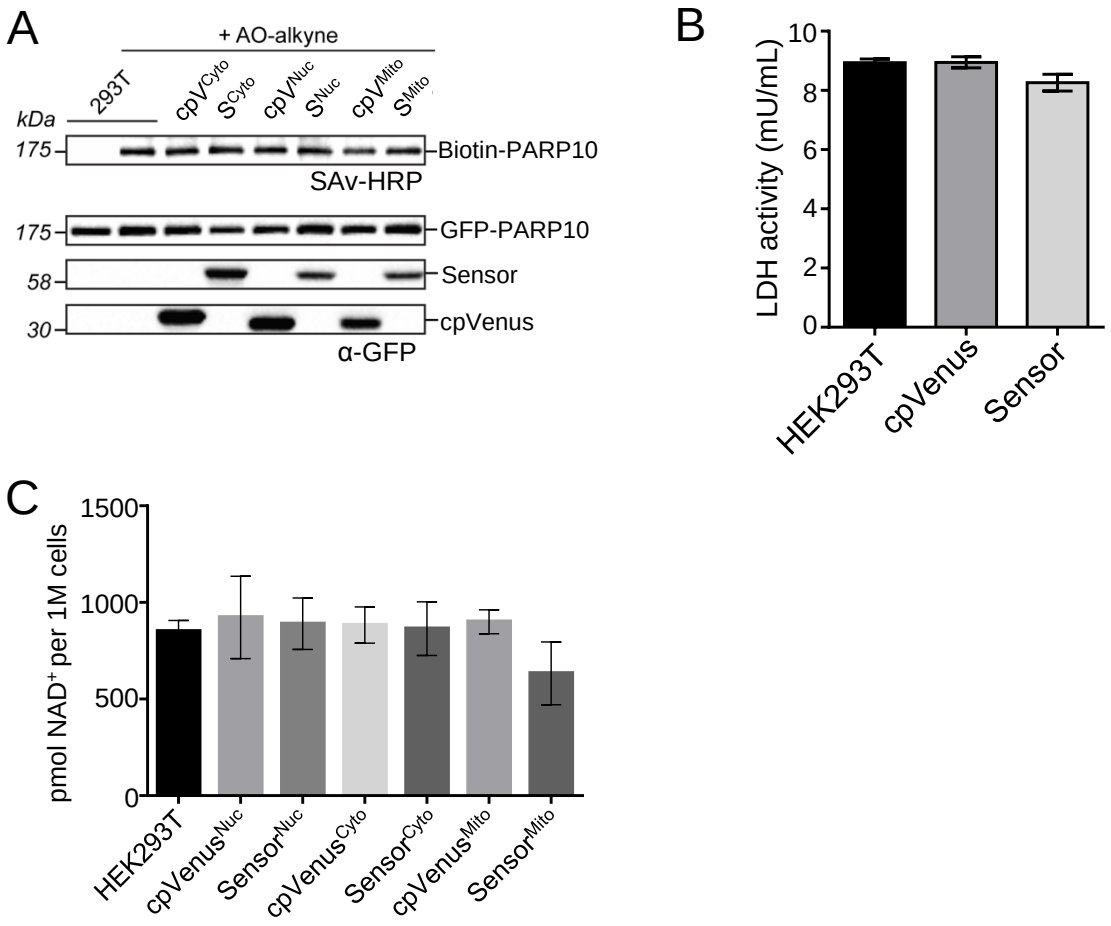

Fig. S10. Expression of sensor does not buffer endogenous NAD⁺.

A) To verify that the sensor itself did not affect free NAD^+ levels in cells, we monitored the activity of the cytoplasmic NAD^+-consuming enzyme PARP10 with an aminooxy-alkyne (AO-alkyne) clickable probe that can detect auto-ADP-ribosylation *(17)*. Expression of the sensors did not affect activity of PARP10, whose K_m for NAD^+ is similar to that of the sensor *in vitro (18)*. Presence of AO-alkyne, representing auto-ribosylation activity of PARP10, was detected with Biotin-azide and Streptavidin-HRP (SAv-HRP).

B) Lactate dehydrogenase (LDH) assay measuring produced NADH for cytoplasmic-localized sensor or cpVenus lines compared to parental HEK293T cells showed no significant change. Mean±SD, n=2, ANOVA, p=0.26.

C) Perchloric acid extraction of whole cell NAD^+ from sensor and cpVenus HEK293T cell lines, measured by HPLC. There were no significant changes. mean±SD, n=3, ANOVA, p=0.21. Estimate for total NAD^+ concentration per cell, if average cellular volume is 1000 fL *(19)* is 350 µM.

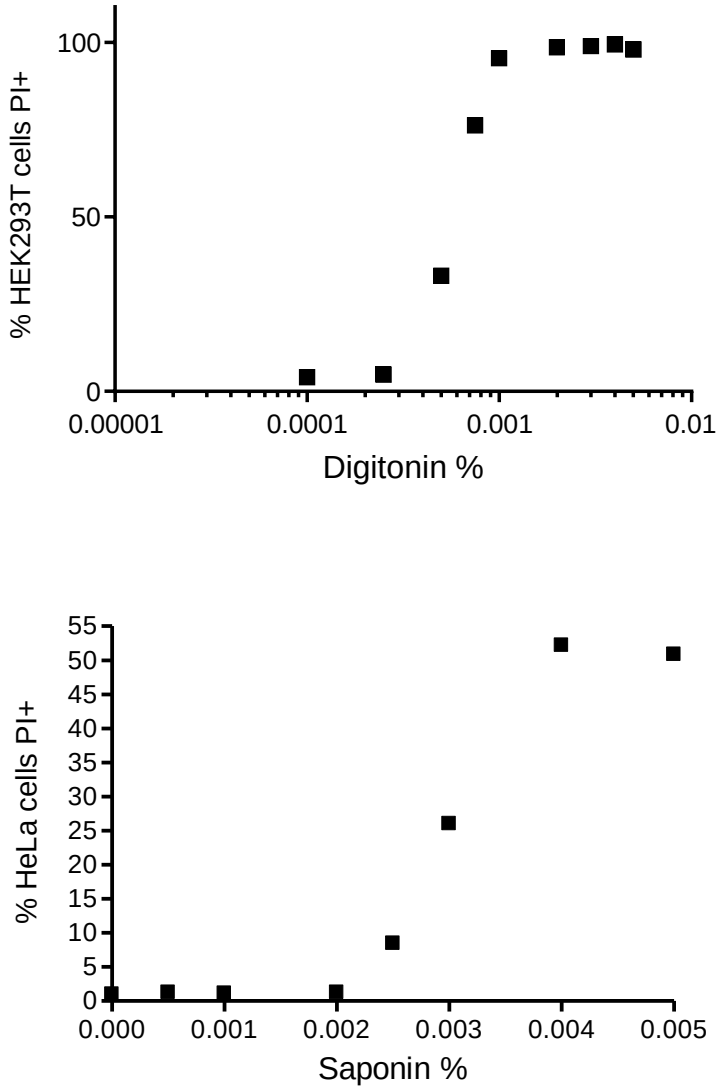

Fig. S11. Concentration of digitonin or saponin required to permeabilize cells. Permeabilization was monitored in real time by the internalization of propodium iodide (PI), and flow cytometry (ex. 561 nm, em. 670/30 nm). HeLa or HEK293T cells were incubated with varying amounts of detergent for 15-30 minutes at room temperature. The percentage of cells taking up PI is shown as a function of detergent concentration.

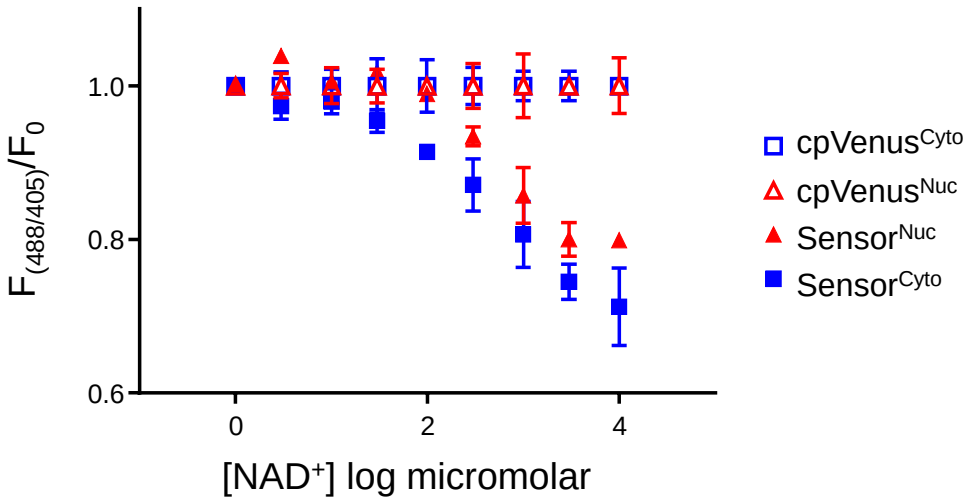

Fig. S12. Relative fluorescence changes in cytoplasmic and nuclear sensors and cpVenus controls.
Clonal populations of HEK293T cells stably expressing either nuclear (Nuc) or cytoplasmic (Cyto) sensor or cpVenus control were permeabilized with 0.001% digitonin and equilibrated with indicated NAD^+ concentrations for 15-30 minutes at room temperature. Relative fluorescence changes are plotted as a function of NAD^+ concentration.

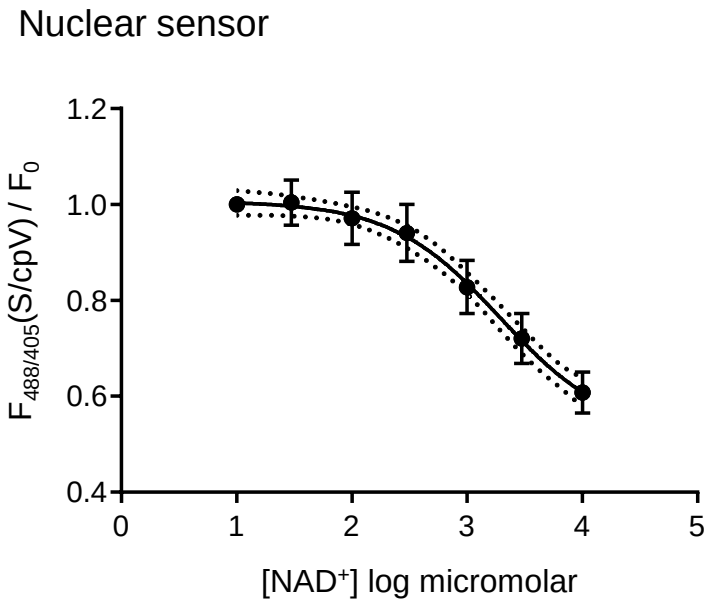

Fig. S13. Calibration curve for the nuclear sensor in HEK293T cells.
HEK293T cells were permeabilized with 0.001% digitonin and equilibrated with indicated NAD^+ concentrations for 15 minutes at room temperature. Fluorescence ratio (488/405 nm) was measured with flow cytometry from the sensor and normalized to the fluorescence from similarly treated nuclear-cpVenus control cells. The mean from 19 independent measurements of the sensor in non-permeabilized cells was interpolated onto the graph to reveal the free nuclear NAD^+ value under homeostasis. Mean±SD, 95% confidence intervals (dotted lines).

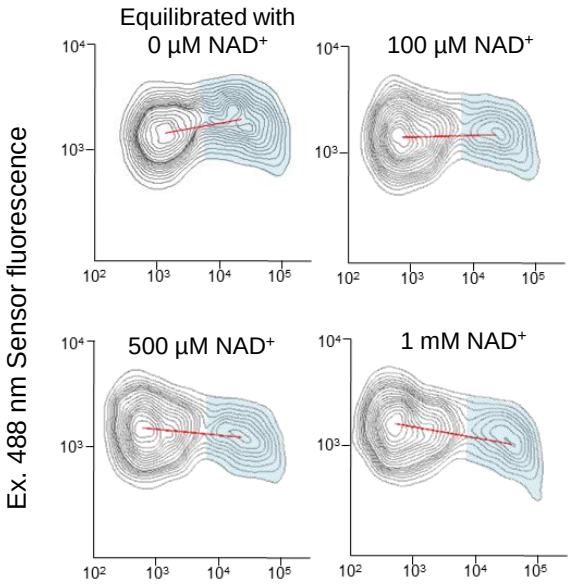

Fig. S14. Fluorescence changes in partially permeabilized HeLa cells.
Cell density plots of HeLa cells partially permeabilized with digitonin (0.0005%) and equilibrated with indicated NAD^+ concentrations. Fluorescence (ex. 488 nm) of the cytoplasmic sensor was evaluated by flow cytometry and permeabilziation was simultaneously monitored by PI internalization (ex. 561 nm). The permeabilized subpopulations are shaded blue and the red line indicates the mode of each sub-population. Equilibration with either 500 µM or 1 mM NAD^+ decreased 488 nm fluorescence of the population. Equilibration with medium containing no external NAD^+ increased fluorescence, likely due to NAD^+ diffusion. Equilibration with 100 µM NAD^+ did not change fluorescence, indicating that cytoplasmic free NAD^+ in HeLa cells approximated this value.

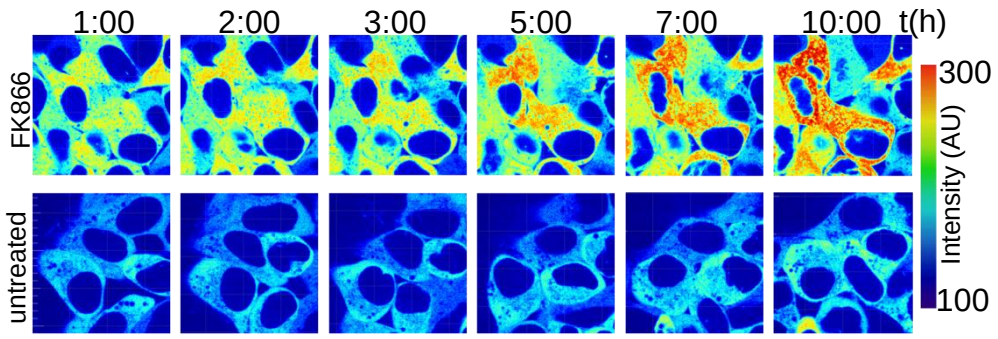

Fig. S15. Inhibition of NAMPT by FK866 depletes steady-state intracellular concentrations of NAD^+.
Representative images from live microscopy of HEK293T cells treated for 10 hours with FK866 (100 µM), ex. 488 nm.

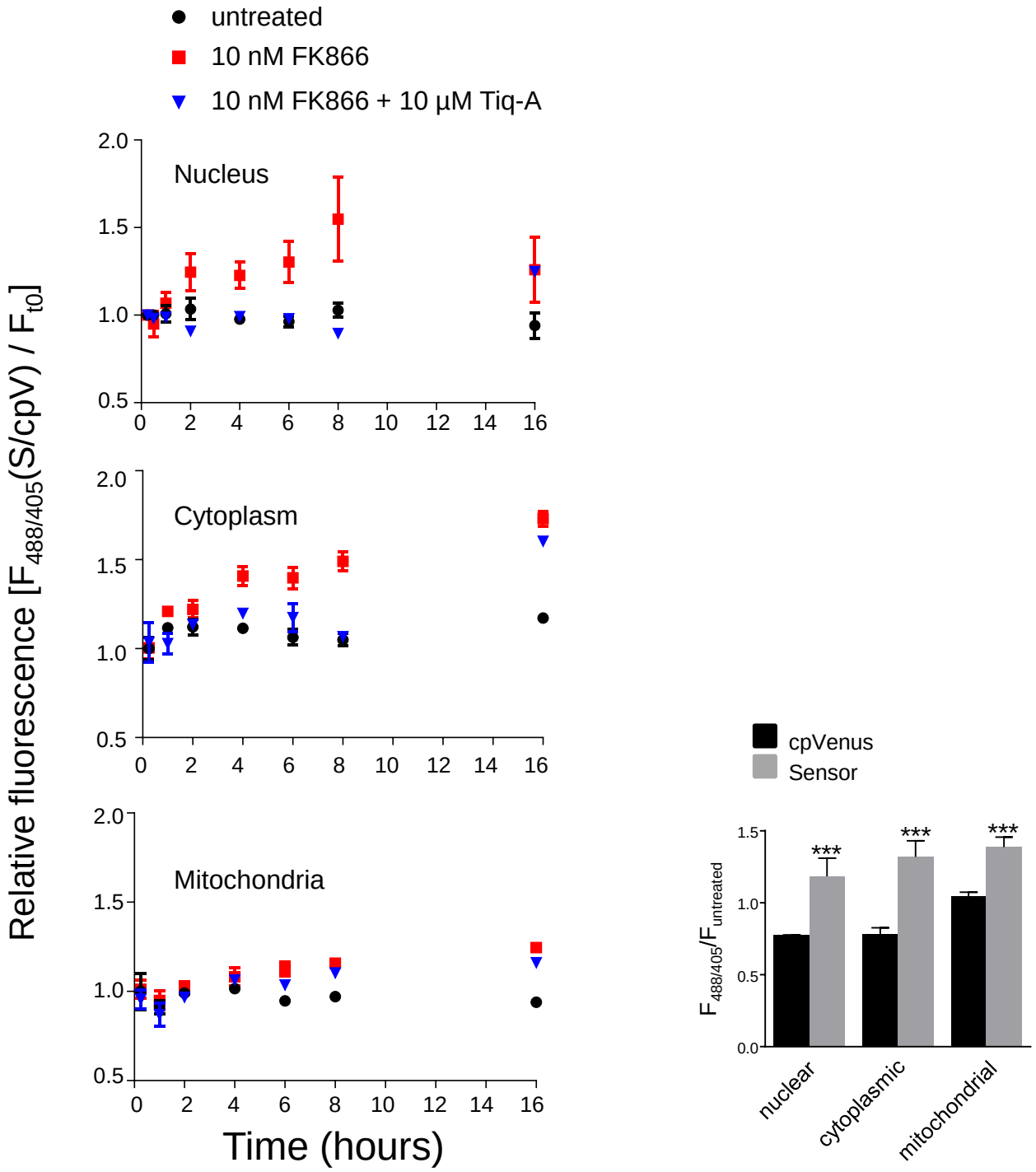

Fig. S16. Relative changes in sensor fluorescence over time.

Left, HEK293T cells expressing localized sensor or cpVenus controls were treated with FK866 (10 nM) and TiqA (10 µM), as indicated. Fluorescence (488/405 nm) per cell was monitored over time using flow cytometry. Values represent Sensor/cpVenus, normalized to time 0. Mean ±SEM, n=5.

Right, Indicated HEK293T cell lines were treated with FK866 (10nM) for 18 hours. Fluorescence measurements (488/405 nm) were normalized to untreated controls. Mean±SD, n=3, ANOVA, Tukey's post-test ***p<0.001.

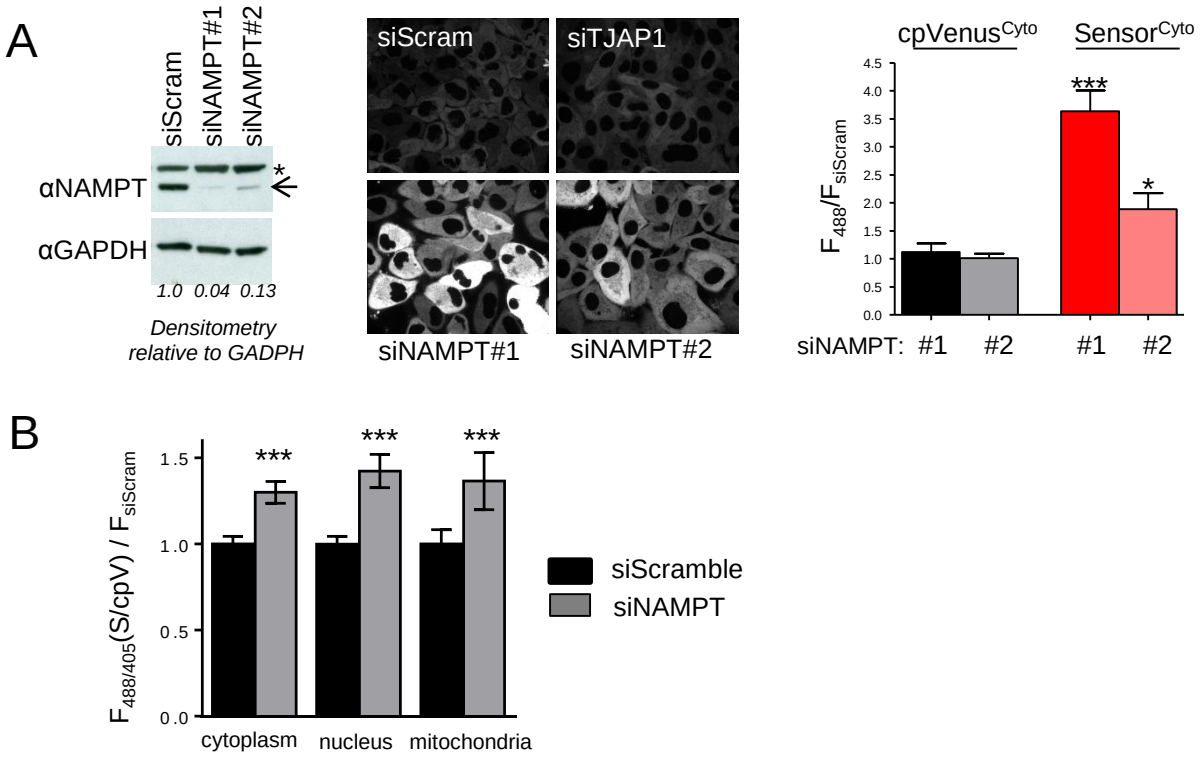

C

	Cytoplasmic			Nuclear			Mitochondrial		
	Mean free NAD^+ (µM)	95% upper CI (µM)	95% lower CI (µM)	Mean free NAD^+ (µM)	95% upper CI (µM)	95% lower CI (µM)	Mean free NAD^+ (µM)	95% upper CI (µM)	95% lower CI (µM)
siScramble	102.8	121.6	87.7	102.8	121.6	87.7	252.7	315.2	204.1
siNAMPT	12.4	15.5	9.7	0.9	1.9	0.0	31.5	37.0	26.6

Fig. S17. Effects of NAMPT depletion on free NAD^+.

A) Left, Efficacy of siRNA depletion of NAMPT (arrow), relative to GAPDH and a scrambled siRNA (siScram). Nonspecific band (*).

Middle, Effect of siNAMPT on fluorescence of cytoplasmic sensor expressed in HeLa cells. Depletion of unrelated protein (siTJAP) served as an additional control.

Right, Quantitation of relative fluorescence (ex. 488 nm) measured by live microscopy. Mean±SEM, 2-way ANOVA $p<0.01$, n=3, Sidak's multiple comparison test, ***$p<0.001$, *$p<0.05$ (right).

B) Depletion of NAMPT in HEK293T cells by siRNA transfection for 72 hours resulted in decreased NAD^+ levels in the cytoplasm, nucleus, and mitochondria. The fluorescence ratio 488/405 nm was measured by flow cytometry and normalized to cpVenus and siScramble controls. REML, mean±SD, n=3, ***$p<0.001$.

C) Calculated mean values for free NAD^+ after NAMPT depletion in HEK293T cells from flow cytometry measurements. 95% confidence intervals are indicated. The change in observed fluorescence was interpolated onto an *in vitro* standard curve.

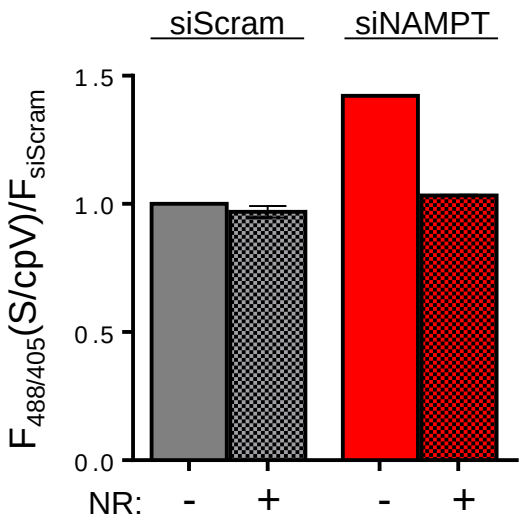

Fig. S18. Effects of NAMPT depletion and NR treatment on cytoplasmic NAD⁺. Ratiometric 488/405 nm measurements were obtained from individual cells using flow cytometry and normalized to cpVenus and siScramble controls. NR, 100-250 µM. mean±SEM, n=2.

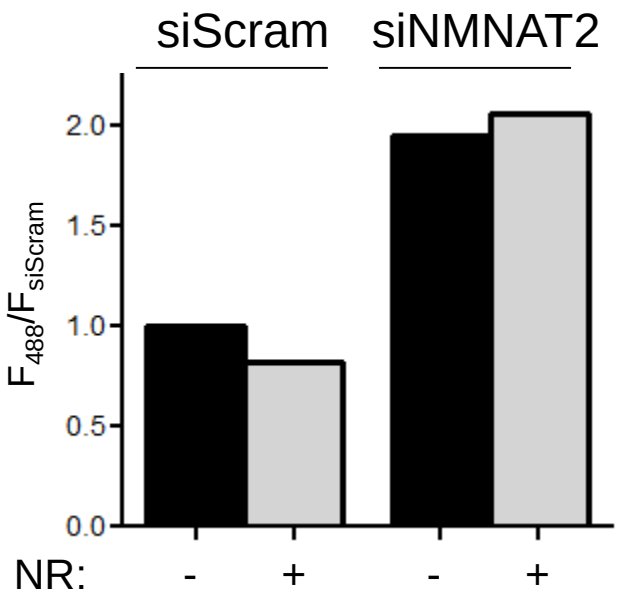

Fig. S19. Nicotinamide riboside (NR) had no direct effect on the fluorescence of the cytoplasmic sensor.

The cytoplasmically-localized sensor in HeLa cells reported a decrease of cytoplasmic NAD^+ following depletion of NMNAT2. NR treatment (1 mM, 24 hours) did not alter the fluorescence (ex. 488 nm) of the sensor when NMNAT2 was depleted.

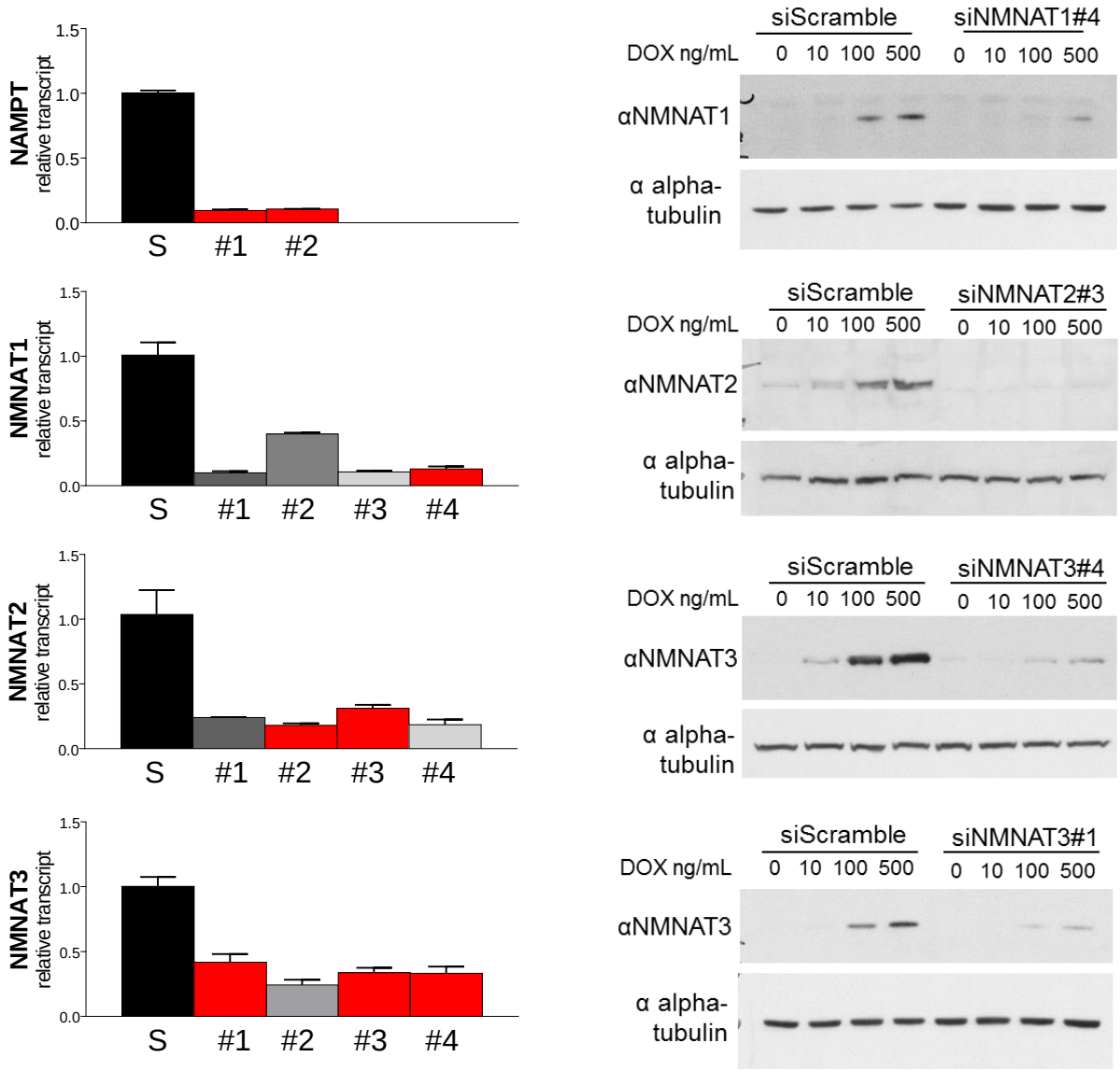

Fig. S20. Validation of siRNAs.
Two to four distinct siRNA sequences were evaluated for knockdown efficiency with both qPCR and Western blotting in HEK293T. Cells were reverse transfected with 25 nM indicated siRNAs or Scramble control (S or Scram) and evaluated 72 hours post-transfection. siRNAs used in this study are highlighted in red and were chosen based on their specific targeting of endogenous transcript with minimal cell toxicity.

Left, Relative levels of endogenous transcripts were quantified with qPCR 72 hours post-transfection of the siRNA.

Right, Due to a lack of antibodies able to recognize endogenous NMNAT1, 2, and 3, we generated doxycyclin-inducible cells lines to ectopically express these proteins. Cell lines were cultured with indicated concentrations of doxycyclin (Dox) for 4 days prior to reverse transfection of the indicated siRNA. Cells were collected for Western blot analysis at 72 hours post-transfection.

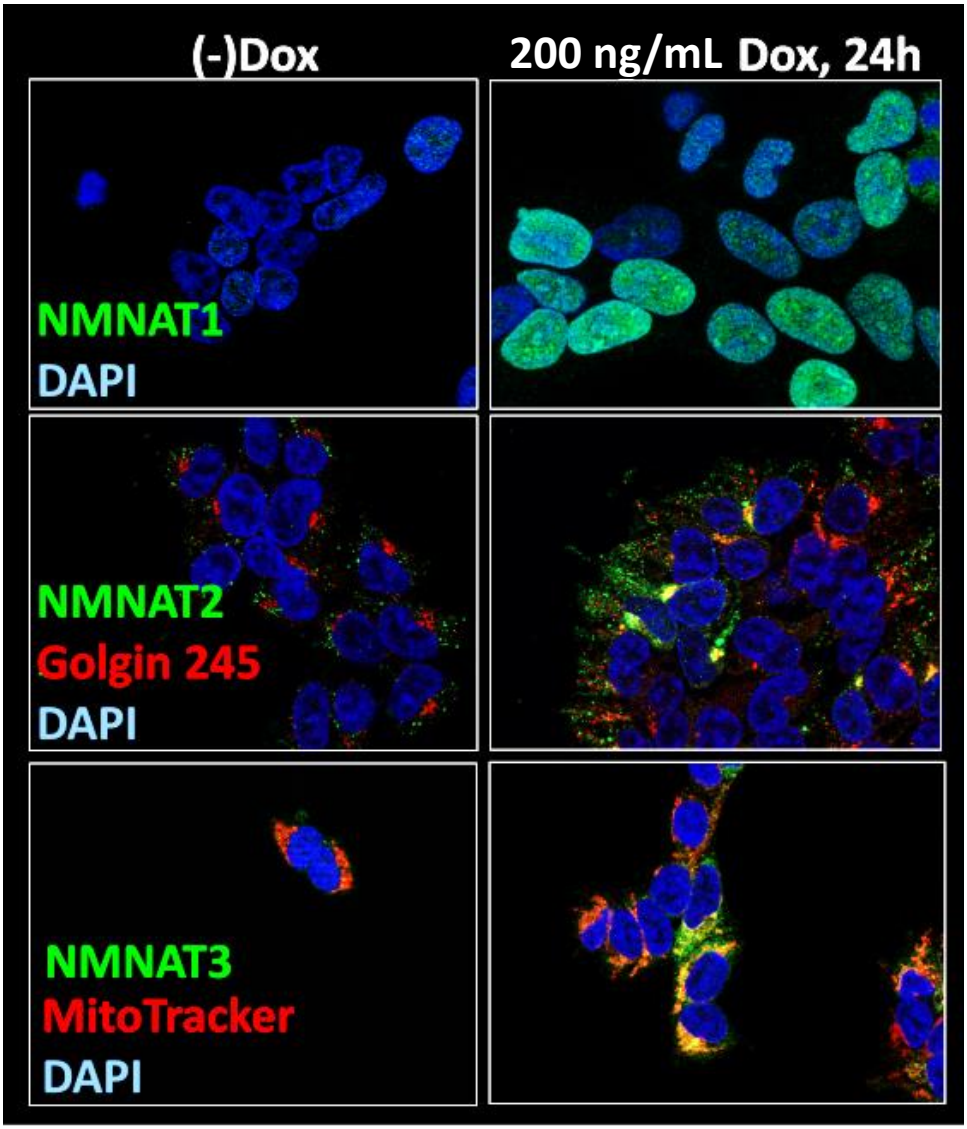

Fig. S21. Localization of ectopically expressed NMNAT enzymes.
Stable HEK293T cell lines were generated using the Tet-ON inducible system (Clontech) to ectopically express either NMNAT1, NMNAT2, or NMNAT3. Cells were induced for 24 hours with 200 ng/mL of doxycyclin, fixed with 4% paraformaldehyde and stained with antibodies recognizing the NMNAT enzymes. Localization was confirmed with DAPI (nuclear), Golgin 245 (trans Golgi apparatus), and MitoTracker CMXRos (mitochodria).

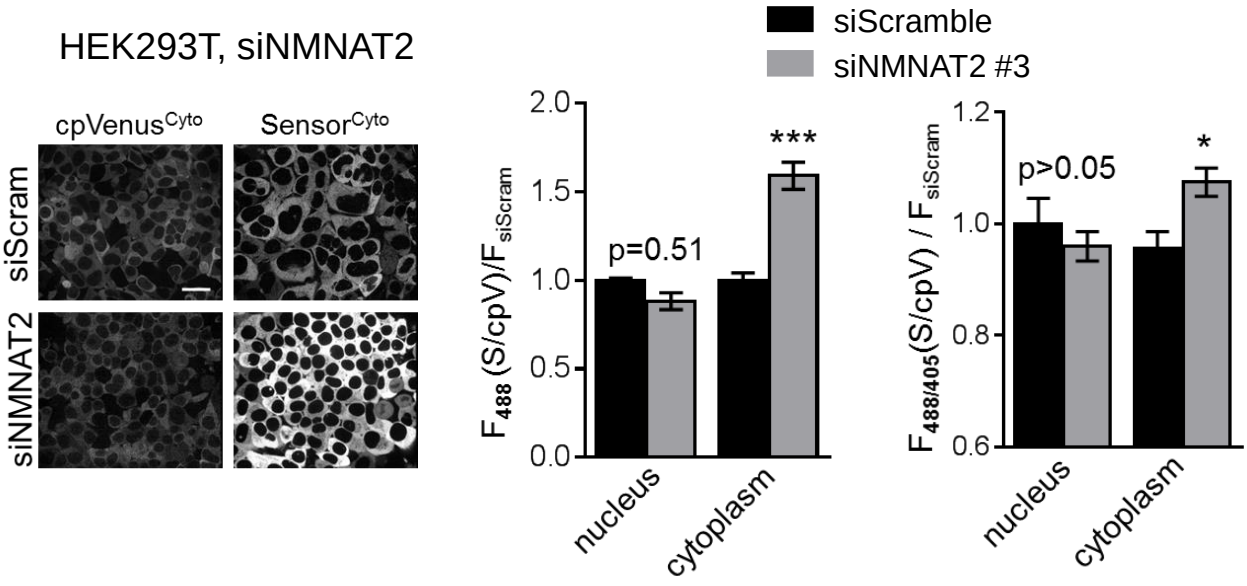

Fig. S22. Contributions of NMNAT2 to the cytoplasmic pool.

Depletion of NMNAT2 resulted in decreased cytoplasmic NAD^+ levels in HEK293T cells but no significant change in nuclear levels.

Left, representative cytoplasmic images, scale bar, 25 μm.

Middle, quantitation of ex. 488 nm fluorescence from nuclear or cytoplasmically-localized sensor (S) and cpVenus (cpV). REML, mean±SEM, n=3, ***p<0.001.

Right, quantitation using flow cytometry analysis of ex. 488/405 nm fluorescence ratio per cell. Sidak's multiple comparison test, mean±SEM, n=4, *p<0.05.

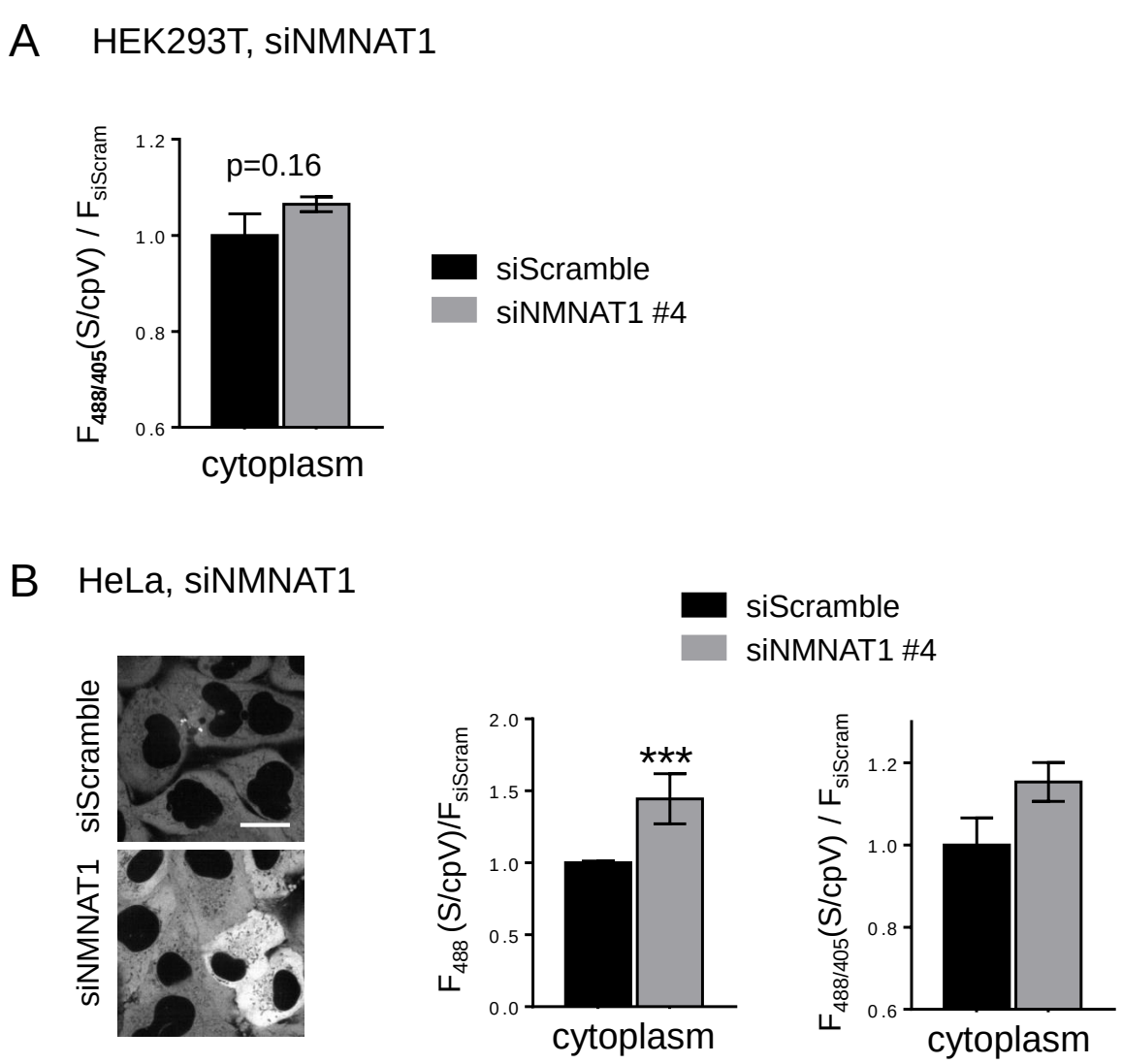

Fig. S23. Contributions of NMNAT1 to the cytoplasmic pool.

A) In HEK293T cells with relatively high NMNAT2, depletion of NMNAT1 was not sufficient to significantly deplete NAD^+ levels in the cytoplasm. REML, mean±SEM, n=3. This contrasts with the observations in HeLa cells in panel B, which express predominantly NMNAT1.

B) In HeLa cells, which express predominantly NMNAT1, the same siRNAs targeting NMNAT1 decreased cytoplasmic NAD^+.

Left, representative images, scale bar, 25 µm.

Middle, quantitation of fluorescence from images using ex. 488 nm. REML, mean±SEM, n=3, ***p<0.001.

Right, quantitation using flow cytometry of 488/405nm fluorescence from individual cells. Mean±SEM, n=2.

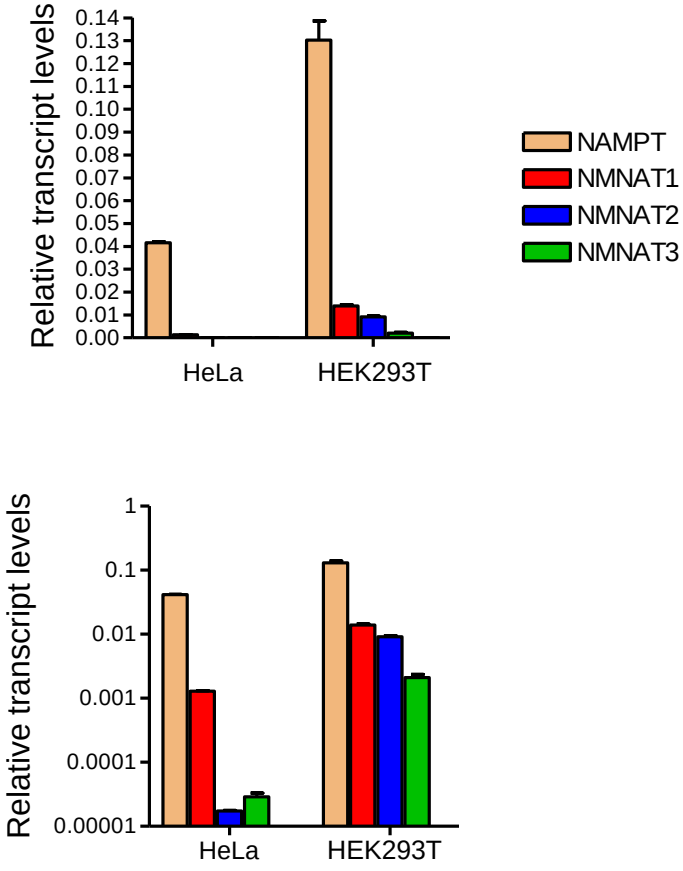

Fig. S24. Relative expression levels of NAD$^+$ biosynthetic enzymes in different cell types.

Quantitative PCR was performed using cDNA from either HeLa or HEK293T cells using validated gene-specific primer sets, as indicated. Relative transcript levels were normalized to GAPDH and either plotted with a linear (top) or logarithmic (bottom) y-axis.

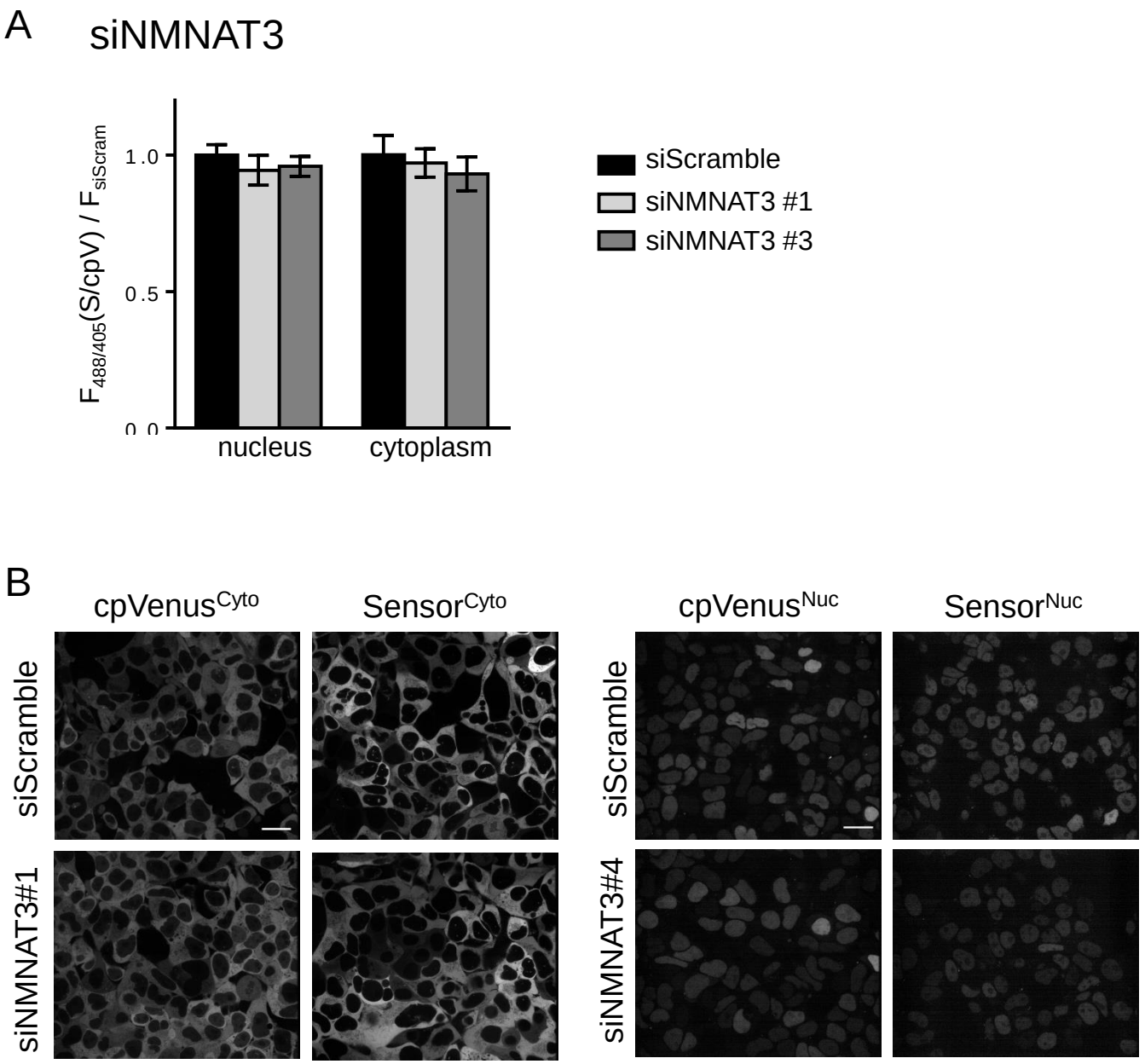

Fig. S25. Depletion of NMNAT3 has no effect on nuclear or cytoplasmic NAD⁺.

A) Depletion of NMNAT3 with different siRNAs had no significant effect on NAD⁺ levels in the nucleus or cytoplasm of HEK293T cells. Fluorescence (488/405 nm) from individual cells was measured by flow cytometry and analyzed using a REML statistical model. Mean±SEM, n=4, p>0.05.

B) Representative images of the sensor's fluorescence in the cytoplasm and nucleus of live cells following depletion of siNMNAT3 with various siRNAs. Scale bar, 25 μm.

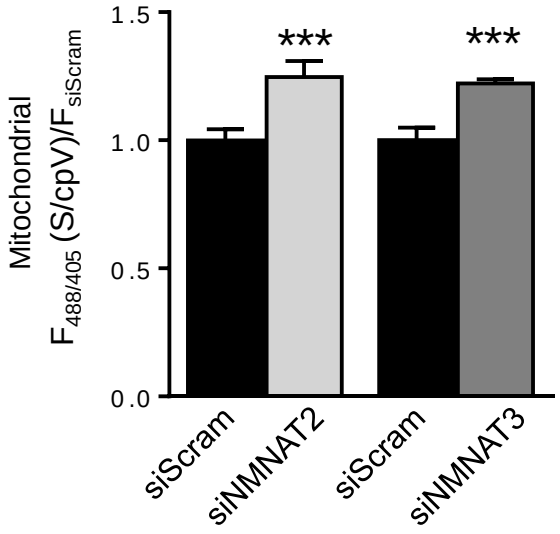

Fig. S26. Depletion of NMNAT2 or NMNAT3 decreased mitochondrial NAD^+ concentrations in HEK293T cells.

HEK293T cells expressing either mitochondrially localized sensor (S) or cpVenus (cpV) were depleted for either NMNAT2 or NMNAT3 using siRNAs. 72 hours post-transfection, cells were analyzed for their individual 488/405 nm ratiometric fluorescence using flow cytometry. Sensor measurements were normalized to cpVenus and siScramble (siScram) controls to obtain fold-change. REML, mean±SEM, n=3, ***p<0.001.

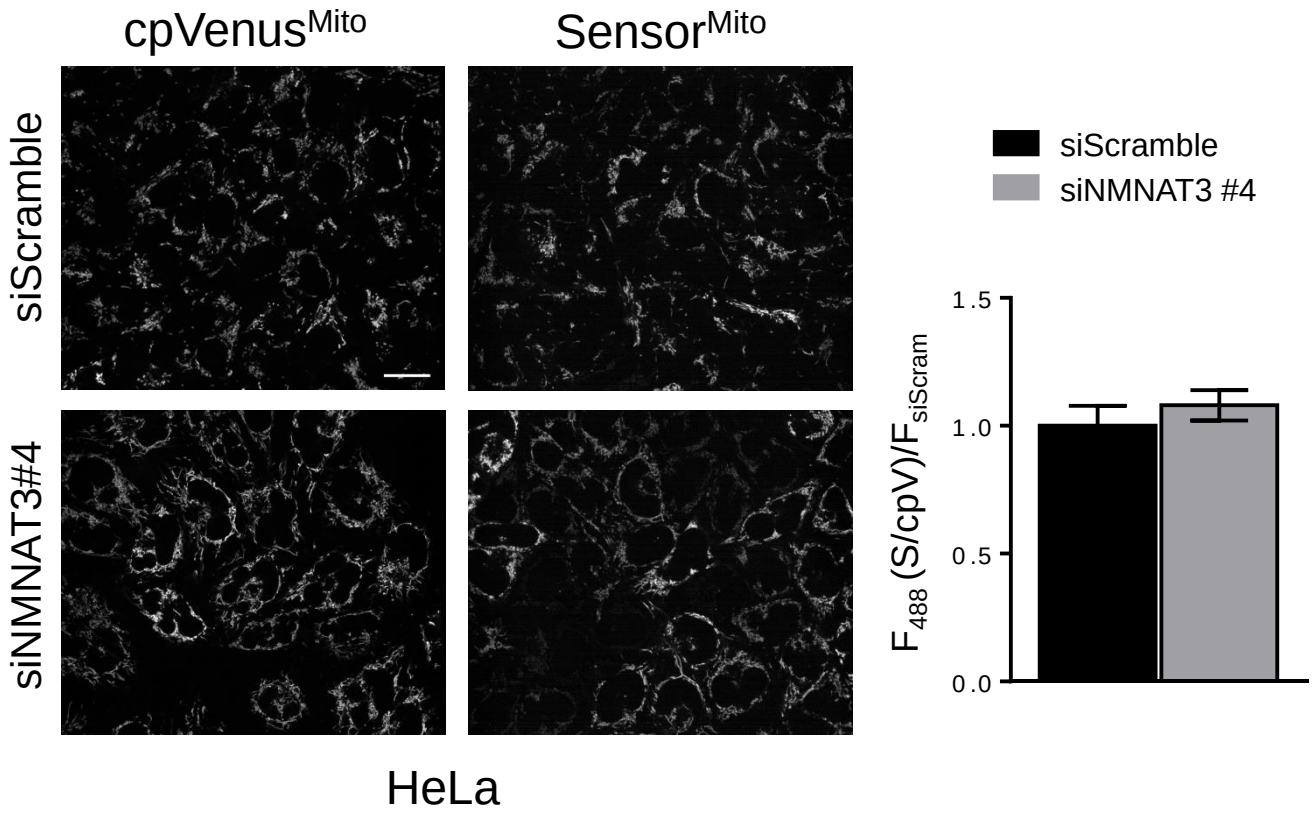

Fig. S27. NMNAT3 depletion has minimal effect on mitochondrial NAD⁺ levels in HeLa cells.

Left, representative images of mitochondria localized sensor (S) or cpVenus (cpV) control. Scale bar, 25 μm.

Right, quantitation of fluorescence (ex. 488 nm). REML, mean±SEM, n=3 p>0.05.

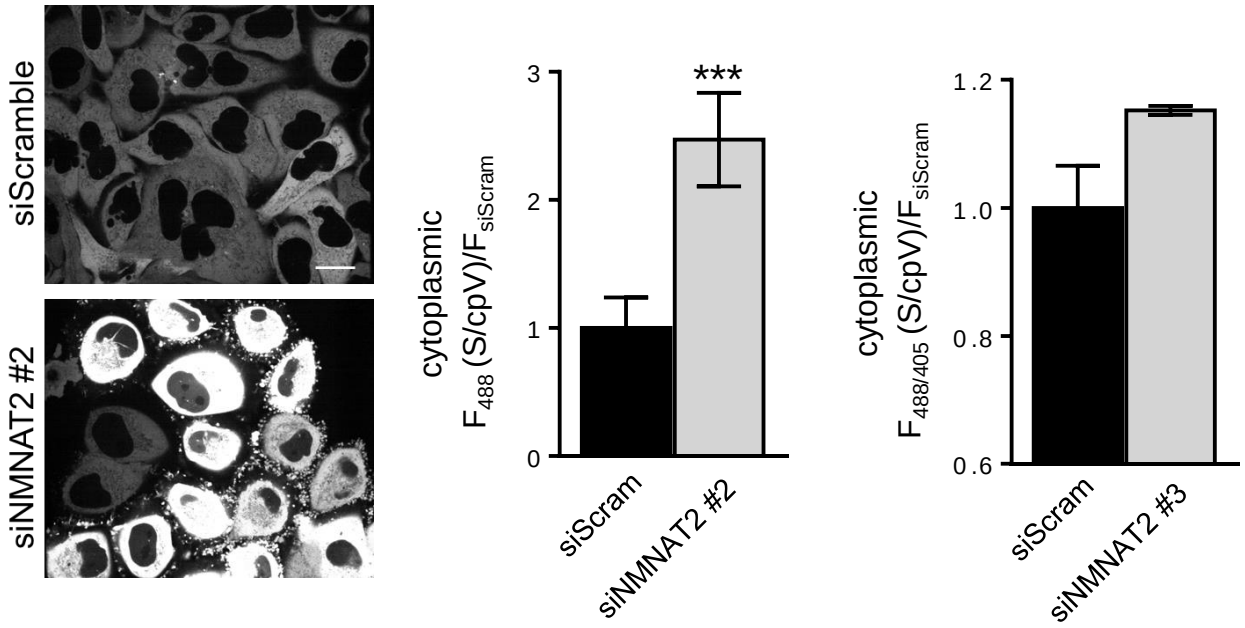

Fig. S28. NMNAT2 is active in HeLa cells.
Depletion of NMNAT2 in HeLa cells resulted in decreased cytoplasmic NAD^+ levels, demonstrating its activity in these cells.

Left, representative images, scale bar 25 μM.

Middle, quantitation of fluorescence, ex. 488 nm, from live microscopy. REML, mean±SEM, n=3, ***p<0.001.

Right, quantitation of individual cell ratiometric fluorescence (488/405 nm) from flow cytometry. Mean±SEM, n=2.